Article:
Sundeep, S., Wang, J. and Griffo, A. (2025) A passive filter for mitigating neutral-point voltage stress in inverter-fed drives. IEEE Transactions on Energy Conversion, 40 (2). pp. 1388-1399. ISSN: 0885-8969

https://doi.org/10.1109/tec.2024.3514136

A Passive Filter for Mitigating Neutral-Point Voltage Stress in Inverter-fed Drives

Shubham Sundeep, Jiabin Wang, *Senior Member, IEEE,* and Antonio Griffo, *Senior Member, IEEE*

***Abstract*—The short turn ON/OFF time and high switching frequencies of the SiC semiconductor devices can lead to several problems such as over-voltage at the machine terminal and in machine windings, increased electromagnetic interference (EMI), and bearing currents. Past studies and standards have proposed numerous EMI filters to mitigate these issues. However, these filters are designed to mitigate the over-voltage at the machine terminals and do not address potentially excessive voltage stress at the star neutral point of a 3-phase winding and may even aggravate this voltage stress. A mathematical model reveals that the voltage stress at the neutral point results from the superposition of voltage waves traveling in different phases. This study proposes an analytical approach, based on impedance measurement, to select the optimal parameters of a cost-effective passive filter to reduce voltage oscillations at the neutral point. Detailed experimental validation is presented showing the benefits of the proposal while resulting in only minimal added losses. Also, the performance of the proposed filter is compared with a commercial dV/dt filter. It is shown that the proposed filter can be used in conjunction with conventional filters to effectively suppress the voltage stress at all locations and reduce conducted EMI.**

***Index Terms*— Adjustable speed drives, common-mode current, common-mode voltage, passive filters, voltage source converter.**

I INTRODUCTION

FAST switching silicon carbide (SiC) semiconductor devices employed in voltage source inverter (VSI) fed drives offer numerous advantages over Si devices based drives, such as higher power density, higher efficiency, reduced harmonic distortion, and improved power/torque controllability. However, fast voltage slew rate and high switching frequency in a SiC inverter excite parasitic capacitive coupling resulting in undesirable issues including (1) voltage overshoot at the machine terminal [1-4] and at the neutral point (Common-mode voltage (CMV)) of the star-connected machine winding [3-4], leading to the potential reduction of the insulation lifetime, (2) common mode (CM) high-frequency (HF) ground return currents which can find a path through the capacitive coupling between the winding and the core of the machine causing conducted electromagnetic interference (EMI) in the electric power system [5], and radiated EMI [6], (3) bearing current as shaft earthing current flowing through the shaft to the grounded driven machinery, or as capacitive discharge current, if the driven machinery is not grounded while the machine core is connected to the ground [5] [7-9]. These problems, except the voltage stress at the neutral point, have been addressed using various mitigation strategies which can be summarized as follows [9-18]:

1) *Change in system configuration:* Shortening the cable length, selecting a cable with higher dielectric loss or the cables with ferrite rings, or opting for different earthing configurations [9] will reduce the overvoltage at the terminal end, although often these are impractical solutions
2) *Installing passive/active filters:* Using a reactor [10] at the inverter output slows down the slew rate of the PWM voltage pulse. Installing a dV/dt filter [11-12] comprising an inductor, capacitor and resistor limits the slew rate of the PWM voltage pulse resulting in reduced voltage stress at the machine terminal at the expense of a significant increase in size, weight, and cost of the drive system. Installing a sinewave filter [13-14] at the inverter output shunts the HF currents to the ground, resulting in sinusoidal voltage at the machine terminals. However, these filters, due to their low cut off frequencies, are bulky and costly as compared to the dV/dt filters and may not offer a significant reduction of common mode voltages. The voltage drop across the bulk inductor in these filters de-rates the converter, reducing voltage utilization and dynamic performance. Installing the motor termination unit at the motor terminals to match the machine impedance with the cable impedance is another solution. However, studies show that this is less effective in suppressing overvoltage [10]. The HF ground return current can be suppressed using a CM transformer [5] [15-16]. However, the transformer is less effective at low modulation index and low fundamental frequency, particularly when the machine operates under no load, or starts and stops frequently. Under these circumstances, the phase currents are less sinusoidal and the low-frequency/peaking phase currents may cause magnetic saturation resulting in a reduction in filter inductance. Active filters [17-18] can be used to mitigate the ground return current and the bearing current. However, these require complex sensing and compensation circuits and result in additional losses.
3) *Multi-level inverters:* These can help in reducing overvoltage at the machine terminal, besides mitigating ground return current and bearing current. However, they increase the complexity, losses, and cost of the drive.

The aforementioned solutions are effective in attenuating the voltage stress at the machine terminal, along with the reduction in HF ground return current and the bearing current. However, mitigations for potentially excessive neutral point

This work was supported by Engineering and Physical Sciences Research Council-EPSRC Grant EP/S00081X/1. For the purpose of open access, the author has applied a Creative Commons Attribution (CC BY) license to any Author Accepted Manuscript version arising. During the development of this paper, Shubham Sundeep, Jiabin Wang, and Antonio Griffo were with The Department of Electronics and Electrical Engineering, The University of Sheffield, Sheffield, S1 3JD UK (e-mail: shubham.sundeep@alumni.iitd.ac.in; j.b.wang@sheffield.ac.uk; a.griffo@sheffield.ac.uk). Shubham Sundeep is now with the National Renewable Energy Laboratory (NREL), Golden, CO, USA.

voltage stress, which has been reported and discussed in [3-4], have not been addressed in the literature.

Standards such as NEMA MG-1:2021 [19], IEC 60034-25:2022 [20], and IEC 61800-8:2010 [21] provide guidance on how to address and reduce the impact of voltage stress on the machine winding when subjected to PWM voltage excitation. However, it is important to note that, the NEMA MG-1:2021 [19] only considers the voltage stress at the machine terminals caused by the PWM voltage pulse that has a rise time greater than 0.1µs. Similarly, the IEC 60034-25:2022 [20], explains the voltage stress at the machine terminals and the contribution of the inverter topologies, filter topologies and the filter on the voltage stress at the machine terminals. However, it does not address the voltage stress at the neutral point. Therefore, the document does not mention any specific filter for its mitigation. The IEC 61800-8:2010 [21] addresses the voltage stress at the machine terminals due to the PWM voltage pulse of rise time as short as 20 ns, wherein, it outlines that this voltage pulse causes uneven voltage distribution among the coils, with the turns closest to the line end experiencing the highest stress, particularly at the shortest rise time. However, the document does not cover voltage stress at the neutral point or recommend any mitigation measures for it. Although this phenomenon has been observed, it is not yet addressed in the standards. Despite this, the document is still an essential reference for working with electrical machines and converters, offering crucial information for safe and effective operation.

In [22], a second-order CM filter is described, comprising a combination of an inductor, capacitor, and resistor. A three-phase coupled inductor is used in between the converter and the machine and a series connected RC circuit is connected between the neutral-point of the winding and the core, and the Y-capacitor. Different from the proposed filter, the filter aims to attenuate CM current, hence, the cut-off frequency is less than 10 kHz. Such a low cut-off frequency results into a bulky and costly solution. The voltage drop across the bulk inductor in these filters results in a reduction of the converter's effectiveness, leading to decreased voltage utilization and dynamic performance. In [23] a CM filter is described which aims to reduce the bearing current. The filter comprises a passive network which is connected between the machine terminals and the mid-point of the DC link. Although, the filter is effective in suppressing voltage stress at the terminal end, it is ineffective in suppressing voltage at neutral point.

In this paper, the voltage stress at the star-neutral point is reviewed and a low-cost passive filter is proposed for mitigating its effect on the lifetime of the insulation. The key contribution of this paper is to attenuate the excessive voltage stress at the neutral point in the following aspects:

1) A comprehensive analysis is presented to illustrate the inefficacy of the conventional filters such as the sinewave filter or dV/dt filter, in attenuating the voltage stress at the neutral point. For experimental verification, the performance of a commercial dV/dt filter is examined experimentally.
2) An RC filter is proposed which is connected between the neutral point of the winding and the machine core or housing (local ground). As no magnetic component is used, the proposed filter is a low-cost compact solution for mitigating voltage stress. Also, it can be suitable as a retrofitting solution without requiring design changes in the machine.

The remainder of the paper is structured as follows. In Section II, the voltage stress at the neutral point is reviewed and the effectiveness of the state-of-art solutions in suppressing the neutral point voltage stress is discussed in Section III. Section IV describes the proposed filter design. The experimental validation is discussed in section V. In section VI, the effectiveness of the Schaffner-designed dV/dt filter is discussed and the concluding remark is made in section VII.

II Neutral Point Voltage Stress

Fig. 1 shows a VSI-fed drive, wherein, the electrical machine is connected to a VSI through a shielded four-wire cable. At the inverter ends, the cable's protective earth (PE) wire is connected to the mid-point of the DC link, and at the machine end, it is connected to the machine core. It should be noted that in a mains-fed drive, although no direct wire connection is made between the earth and the inverter, a low impedance path for the high frequency CM currents exists through the front-end rectifier and earthed neutral point of the feed transformer. In an IT (isolé terre) grounding system, such as those in electrified transport systems, a low impedance path is provided through the Y-capacitors of an EMC filter which is necessary for compliance with relevant EMC standards [24-25]. Conventionally, the neutral point voltage, represented as v_{Nf} in Fig. 1 is the voltage between the star-connected neutral point and the core of the machine. Assuming the machine has a balanced three-phase load and the high frequency behavior of the machine windings is ignored, the neutral point voltage in steady state can be expressed mathematically as;

$$v_{Nf} = \frac{v_{Af}+v_{Bf}+v_{Cf}}{3} \quad (1)$$

where, v_{Af}, v_{Bf}, and v_{Cf} are the voltages measured at the machine phases with respect to (w.r.t) the machine core. Assuming, the

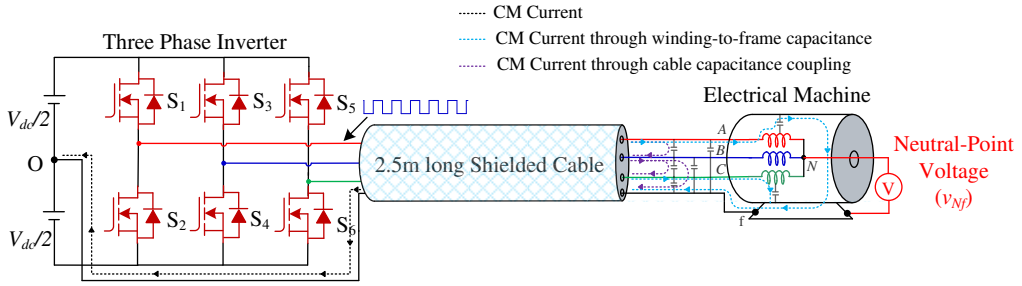

Fig. 1. Schematic of a conventional electric drive with an electrical machine connected to the VSI.

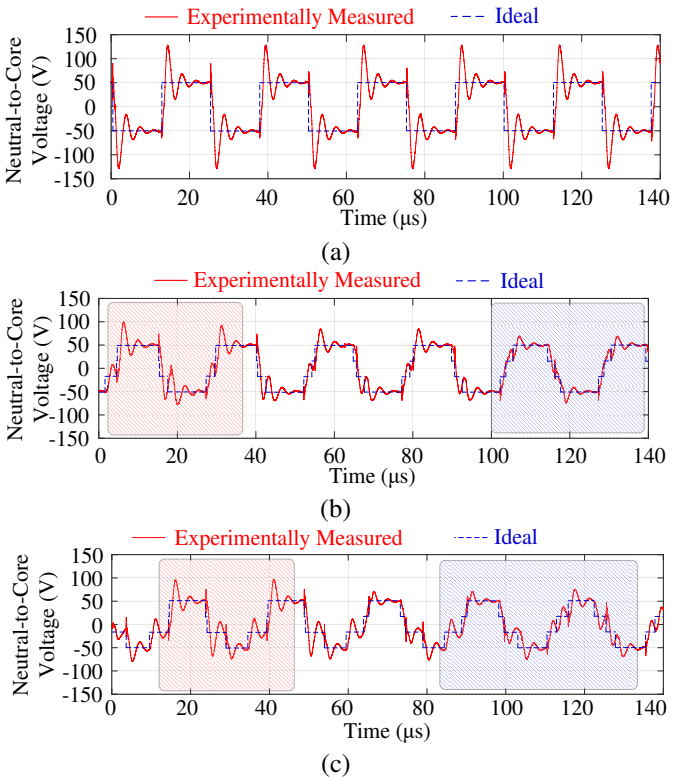

Fig. 2. Experimentally measured neutral point voltage (red traces) at 100V DC link voltage and three modulation indexes (m); (a) m = 0.01, (b) m = 0.3, (c) m = 0.5.

cable is ideal, (1) can be written as:

$$v_{Nf} = \frac{v_{Ao}+v_{Bo}+v_{Co}}{3} \tag{2}$$

where, v_{Ao}, v_{Bo}, and v_{Co} are the pole voltages measured w.r.t. the mid-point ('o') of the DC link. In a 2-level inverter, the neutral point voltage will be a six-step voltage varying within $\pm V_{DC}/2$, if the VSI is controlled by sinusoidal pulse width modulation (SPWM) or space vector pulse width modulation (SVPWM) technique [24]. In Fig. 2, this is represented by a blue trace at three modulation indexes. However, equation (2) holds only if the HF current flowing through the capacitive coupling between the stator winding and the core is neglected. As an illustration, the experimentally measured neutral point voltage (v_{Nf}) for three values of the modulation index, is represented by red trace in Fig. 2. During the experiment, the 2010 Toyota Prius hybrid vehicle 60 kW PMSM is used [27] and is excited by a SiC inverter with a voltage rise time of 20 ns at 40 kHz switching frequency. Evidently, (2) fails to represent the HF oscillatory components in the voltage waveform.

At a low modulation index (m = 0.01), in Fig. 2 (a), the switching at all three phases occurs nearly simultaneously. Consequently, a consistently large peak can be observed at every switching instant. At a higher modulation index (m = 0.3 or 0.5), during the red-shaded intervals in the left-hand sides of Fig. 2 (b-c), two of the three phases switch simultaneously, thereby, the voltage peaks are higher as compared to the blue-shaded intervals in the right-hand sides of Fig. 2 (b-c), wherein, all the three phases switching events are separated by a sufficient time for the oscillation to dampen. Thus, peak voltage

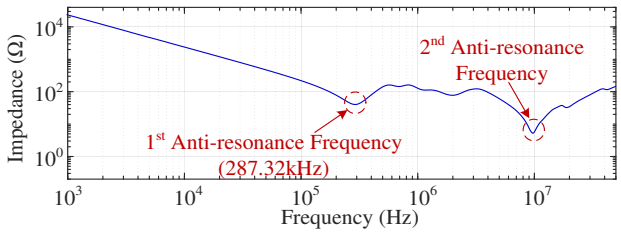

Fig. 3. Experimentally measured CM impedance of the machine winding.

stress depends on the dwell time between the switching events at the phases, which, in Fig. 2, is a function of the modulation index. The dwell times also vary with the phase angle of the voltage vector periodically at every 60 electrical degrees.

This oscillatory mode occurs because of the resonance within the machine winding. Fig. 3 shows the CM impedance measured at the terminal of the machine, wherein, the 1st anti-resonance of the winding is at 287.32 kHz, which corresponds to the frequency of the voltage oscillations at the neutral point. The above analysis is discussed comprehensively in [3-4]. These voltage oscillations are a result of superposition of transverse electromagnetic (TEM) voltage waves which are elicited due to three-phase voltage excitation. These waves travel along the three-phase winding and superpose to result into a standing wave at the neutral point. These travelling waves can be expressed as [3-4];

$$v_{A_{ac}}(t) = v_{A_m}\sqrt{1+\left(\frac{\zeta}{\omega}\right)^2}\, e^{-\zeta(t-\tau_A)} sin\left(\omega(t-\tau_A) + tan^{-1}\left(\frac{\zeta}{\omega}\right) - \frac{\pi}{2}\right) \tag{3}$$

$$v_{B_{ac}}(t) = v_{B_m}\sqrt{1+\left(\frac{\zeta}{\omega}\right)^2}\, e^{-\zeta(t-\tau_B)} sin\left(\omega(t-\tau_B) + tan^{-1}\left(\frac{\zeta}{\omega}\right) - \frac{\pi}{2}\right) \tag{4}$$

$$v_{C_{ac}}(t) = v_{C_m}\sqrt{1+\left(\frac{\zeta}{\omega}\right)^2}\, e^{-\zeta(t-\tau_C)} sin\left(\omega(t-\tau_C) + tan^{-1}\left(\frac{\zeta}{\omega}\right) - \frac{\pi}{2}\right) \tag{5}$$

where, ζ and ω are damping factor and damped frequency of oscillation respectively, τ_A, τ_B and τ_C represents the instants at which the voltage waves arrives at the machine winding terminals, and v_{Am}, v_{Bm} and v_{Cm} are the voltage waves amplitude in phase A, B and C respectively. The DC component of the voltage wave is a quasi-square wave whose peak amplitude varies between $\pm V_{DC}/2$, and depends on the switching states of the phases. For instance, if S_z (where, z = A, B, C) is the switching state of a phase; such that, S_z = 1 when the top switch is ON and S_z = 0 when the bottom switch is ON, then the DC component is;

$$v_{z_{dc}}(t) = \begin{cases} \frac{V_{DC}}{6}; & S_z(t) = 1 \\ -\frac{V_{DC}}{6}; & S_z(t) = 0 \end{cases} \quad \forall \;\; z = A, B, C \tag{6}$$

where, V_{DC} is the DC-link voltage. Thus, the neutral point voltage (v_{Nf}) with respect to the core is expressed as;

$$v_{Nf}(t) = \underbrace{\left(v_{A_{ac}}(t) + v_{A_{dc}}(t)\right)}_{v_A} + \underbrace{\left(v_{B_{ac}}(t) + v_{B_{dc}}(t)\right)}_{v_B} + \underbrace{\left(v_{C_{ac}}(t) + v_{C_{dc}}(t)\right)}_{v_C} \tag{7}$$

Thus, the neutral point voltage is a superposition of the three travelling waves and can be expressed mathematically using (3-

7). Notably, the mathematical model does not account for the voltage oscillations due to previous switching. It is assumed that the voltage oscillations dampen out prior to the arrival of the next switching event. However, if the switching event arrives before the voltage oscillations damp out, the voltage wave can be expressed as:

$$v_{z_{ac}}(t) = \underbrace{v_{z_m}\sqrt{1+\left(\frac{\zeta}{\omega}\right)^2}\, e^{-\zeta(t-\tau_z)} sin\left(\omega(t-\tau_z)+tan^{-1}\left(\frac{\zeta}{\omega}\right)-\frac{\pi}{2}\right)}_{Forced\ Response}$$

$$+\underbrace{v_{z_0}\sqrt{1+\left(\frac{\zeta}{\omega}\right)^2}\, e^{-\zeta(t-\tau_z)} sin\left(\omega(t-\tau_z)+tan^{-1}\left(\frac{\zeta}{\omega}\right)+\phi_{z_0}-\frac{\pi}{2}\right)}_{Natural\ Response}$$

$$\forall\ z = A, B, C \qquad (8)$$

where, v_{z_0} and ϕ_{z_0} is the amplitude and phase of the sinusoidal voltage oscillation due to previous switching event. Thus, the voltage oscillations in each phase is a combination of the forced response which is the voltage oscillation arising due to current switching event, and the natural response which is the damped voltage oscillation due to previous switching event.

The mathematical model (3-8) is validated by measuring the damping factor (ζ) and the damped frequency of oscillation (ω) experimentally. These parameters are measured at the low modulation index, wherein, switching event arrives at all the phases simultaneously. Using the experimentally measured parameters as, $\zeta = 3.75\times10^5$ s^{-1} and $\omega = 1.805\times10^6$ rads^{-1}, the prediction for the neutral point voltage is illustrated in Fig. 4 alongside the experimentally measured voltage for comparison.

It is noteworthy that, in a SVPWM technique, the dwell time of the active space vectors (τ_A-τ_B and τ_B-τ_C) depends on the modulation index (m), switching frequency, and phase angle (θ). Consequently, the voltage distribution is a function of these factors, which is illustrated in Fig. 2.

Often, it is advised that shortening the cable length reduces the peak voltage stress at the machine terminals [9]. However, the neutral point oscillatory mode is an intrinsic characteristic of the machine and therefore it is independent of the cable length. By way of example, Fig. 5 compares the neutral point voltage measured experimentally between two different cable lengths (l_c), (a) l_c = 0.5 m, (b) l_c = 2.5 m at the DC link voltage of 550 V, a voltage rise time of 20 ns and switching frequency of 40 kHz. In both cases, the neutral point voltage remains the same whereas, the peak-to-peak machine terminal voltage is increased from 1150 V to 1300 V when the cable length is increased from 0.5m to 2.5m.

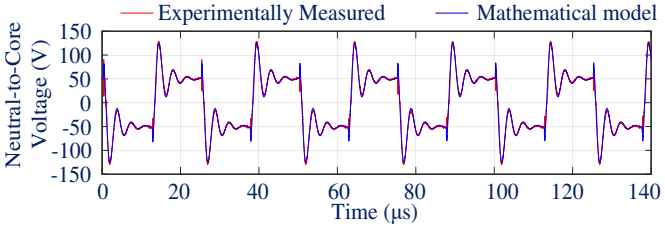

Fig. 4. Comparison between the neutral point voltage predicted through the mathematical model and the experimentally measured voltage at 0.01 modulation index and 100 V DC link voltage.

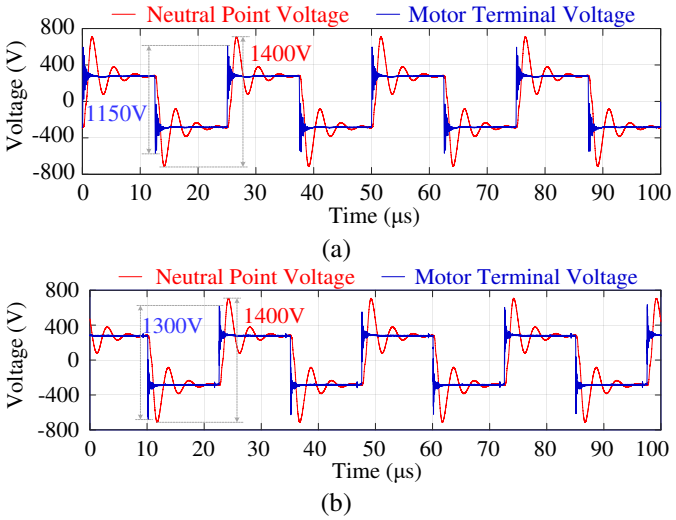

Fig. 5. Experimentally measured neutral point voltage at different cable lengths (l_c); (a) l_c = 0.5 m, (b) l_c = 2.5 m.

The solutions proposed in the literature [10-18] are aimed at attenuating the voltage stress at the terminal voltage and the resultant CM current while the peak voltage stress at the neutral point has not been addressed. Likewise, passive filters such as line reactors, sinewave filters, dV/dt filters, or CM choke proposed in the literature are intended to attenuate the voltage stress at the terminal end of the machine. For effective attenuation of the CM current, the oscillatory nature of the voltages in machine windings must be understood as it influences the leakage current through the machine insulation.

The following study proposes a low-cost filter, which is specifically designed to attenuate the neutral point voltage stress, which, if undamped, may result in costly downtime due to premature failure of the insulation.

III Effect of Conventional Passive Filters

Conventional passive filters, such as a sinewave filter or dV/dt filter are effective in alleviating the voltage stress at the machine terminal. Being relatively low cost, easy to install, and a reliable solution, they are widely used in industry [10-14]. The filter components are selected to mitigate terminal voltage. However, in certain instances, these filters can aggravate the neutral point voltage stress. The following discussion illustrates the effect of these filters on the neutral point voltage stress.

A. Effect of Sinewave Filter

The Sinewave filters are installed in the VSI-fed drives to convert the HF square wave voltage pulse into sinusoidal excitation. Therefore, the resonance frequency of the filters should be selected between the fundamental frequency and the switching frequency. For better attenuation of the HF voltage pulse, it is advised that the resonance frequency should be an order of magnitude less than the switching frequency [13]. By way of example, a MATLAB based model of sinewave filter installed in a VSI-fed drive is developed with filter parameters as; L_f = 1.2 mH, R_f = 0.3 Ω , C_f = 0.845 μF, and 5 kHz resonance frequency [13]. The model is excited through an ideal voltage source with a pulse rise time equal to 20 ns. The DC link voltage

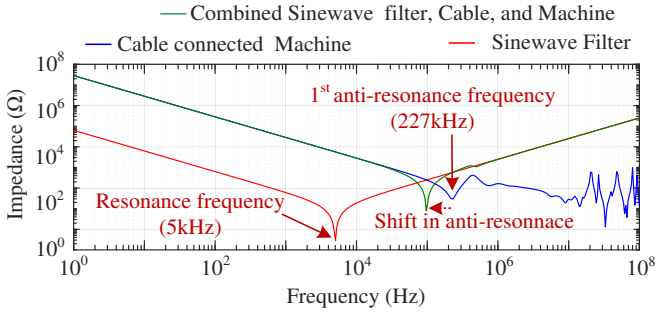

Fig. 6. CM impedance measurement with sinewave filter.

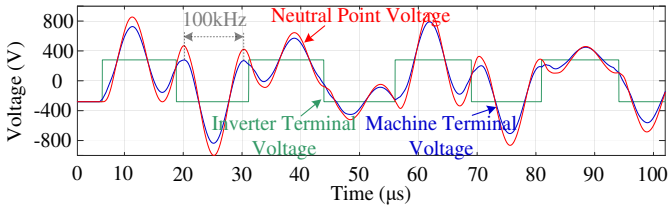

Fig. 7. Voltage stress within the winding with Sinewave filter.

is 550 V. The electrical machine connected with the shielded cable is represented using an HF behavioral model [3].

The CM impedance of the filter is compared with those of the cable and machine, and the combined filter, cable, and the machine in Fig. 6. The filter resonates at 5 kHz, whereas the cable connected machine resonates at 227 kHz. Due to the low resonance frequency of the filter, the anti-resonance frequency of the combined filter, cable, and machine shifts to 100 kHz, with decreased impedance and damping. As a result, the neutral point voltage oscillates at 100 kHz, as illustrated in Fig. 7. The filter reduces the impedance at the anti-resonance frequency of the combined system, consequently, aggravating the voltage oscillations at the neutral point, as shown in Fig. 7.

However, as shown in [13-14], due to the increased impedance at frequencies above 1 MHz the 2nd anti-resonant mode of the cable-machine system is eliminated and consequently, terminal voltage oscillations are damped. In summary, while sinewave filters successfully minimize voltage stress at the machine terminals, their low cutoff frequency can exacerbate stress at the neutral point. This increased stress may negatively impact the integrity of the main-wall insulation near the neutral point of the winding.

B. Effect of dV/dt Filter

The dV/dt filters limit the slew rate of the voltage pulse impinging the machine terminal, by increasing the rise time of the pulse, thereby, reducing the voltage stress at the machine terminals. A MATLAB Simulink-based model of dV/dt filter installed VSI-fed drive is illustrated in Fig. 8, where the filter's parameters are adapted from [11]. The CM impedance of the filter is compared with those of the cable-connected machine and the combined filter, cable, and machine in Fig. 9. The corner frequency of the filter, 490 kHz, is higher than the 1st anti-resonance frequency (227 kHz) of the combined cable and machine. Therefore, the 1st anti-resonance mode of the combined filter, cable, and machine is unchanged. As a result, the neutral point voltage oscillations remain undamped as demonstrated in Fig. 10. However, due to increased impedance

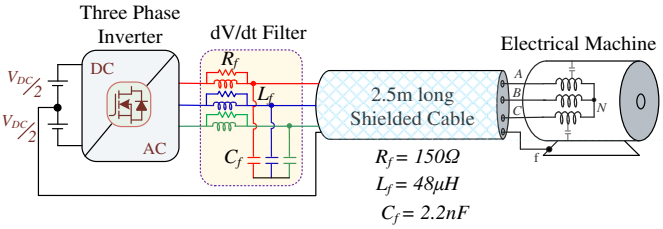

Fig. 8. Schematic of VSI-fed drives with dV/dt filter [11].

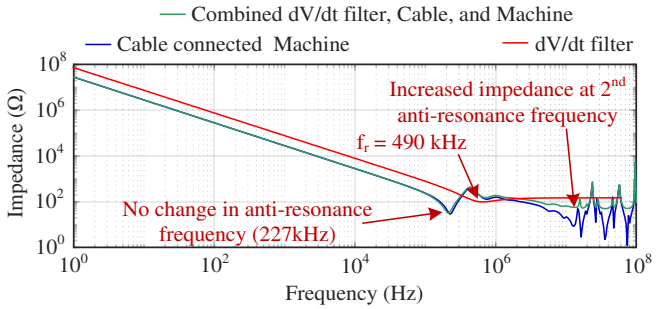

Fig. 9. CM impedance measurement with dV/dt filter.

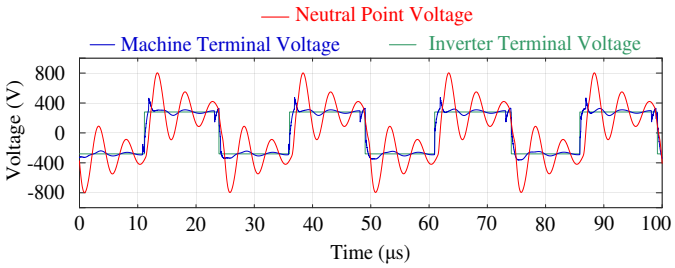

Fig. 10. Voltage stress within the winding with dV/dt filter.

and damping around the 2nd anti-resonance frequency of the combined system, the terminal voltage oscillations are significantly attenuated.

However, a properly designed filter with a resonance frequency lower than the anti-resonance frequency will provide some degree of effectiveness in voltage suppression, as extensively discussed in section VI.

IV Proposed Passive Filter Design

Fig. 11 shows the schematic of the proposed passive filter, wherein, a series resistance and capacitance are connected between the neutral point and the core of the machine. At the neutral point, the capacitance provides a low impedance path for the HF oscillatory voltage, whereas, the resistance dissipates energy associated with the neutral point oscillations and limits the current through the capacitor. Higher-order filters are also possible at the expense of increased circuit complexity. However, the proposed filter is effective in the attenuation of the neutral point voltage stress with minimum components count and losses.

As discussed in the previous section, voltage oscillations occur due to the anti-resonance phenomenon. The winding offers low impedance and low damping at the anti-resonance frequency, thereby, resulting in voltage oscillations. The RC filter is designed to provide increased damping at this frequency.

The parameters of the filters are evaluated based on the

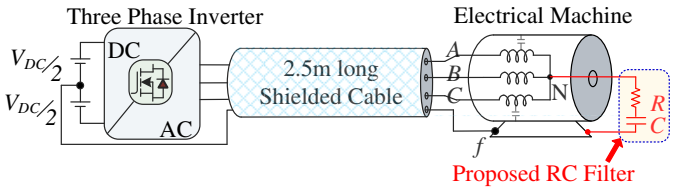

Fig. 11. Proposed passive filter connected between the neutral point and the core of the machine.

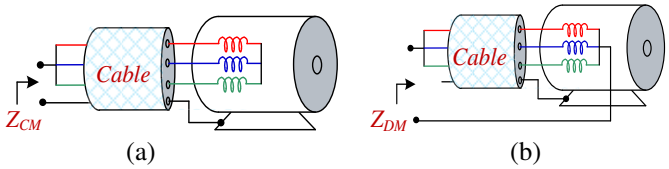

Fig. 12. Experimental impedance measurements used for filter design; (a) CM impedance, (b) DM impedance.

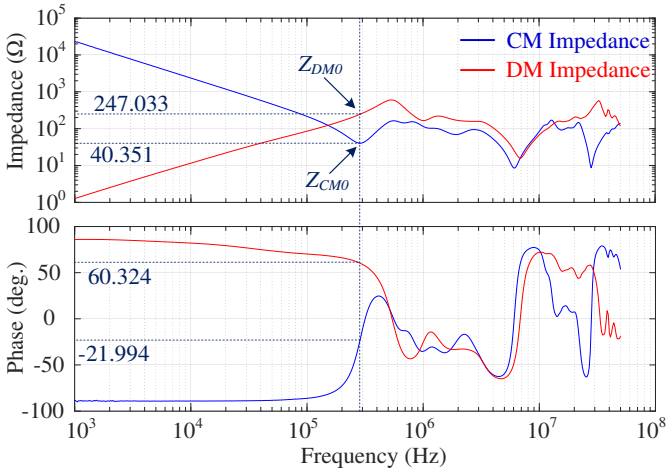

Fig. 13. Experimental measured CM and DM impedance of the cable connected machine winding.

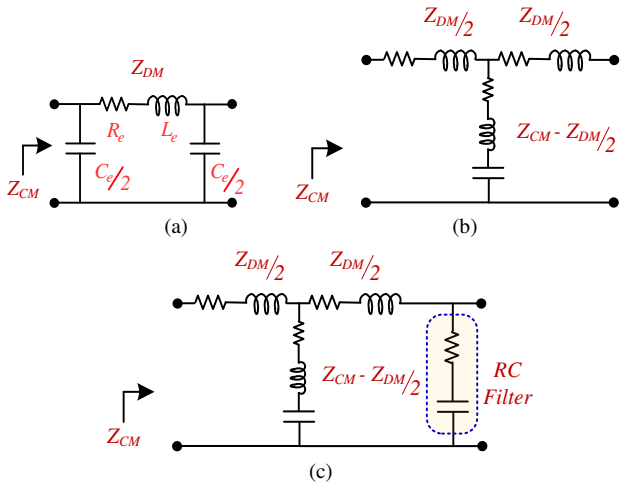

Fig. 14. Frequency-dependent equivalent circuit of the machine based on CM DM impedance measurement, (a) Π circuit, (b) Γ Circuit, (c) Equivalent circuit with a proposed RC filter.

measured impedance of the cable connected winding at anti-resonance frequency. Fig. 12 shows the schematic of the CM and differential-mode (DM) impedance measurements and the measured impedances are shown in Fig. 13. From Fig. 13, the CM and DM impedance at the 1st anti-resonance frequency is

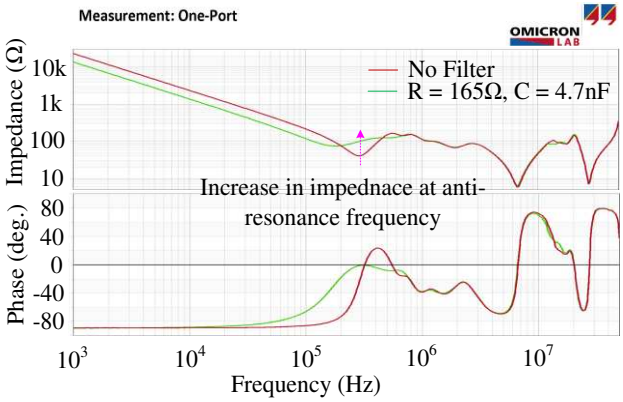

Fig. 15. Experimentally measured CM impedance of the cable connected machine winding illustrating the effect of the proposed filter.

denoted as Z_{CM0} and Z_{DM0} respectively. These measurements can be modelled using an equivalent Π and Γ circuit with frequency-dependent parameters, as illustrated in Fig. 14 (a-b). The equivalent capacitance (C_e) indicates the capacitance between the winding and the core of the machine which is proportional to the relative surface area between windings and stator core. The larger the capacitance, e.g. for machines of larger size, the lower the 1st anti-resonance frequency. On the other hand, the equivalent inductance (L_e) represents the series inductance of the cable and the machine winding which increases with the number of turns per phase, leading to higher DM impedance. The equivalent inductance and the capacitance can be evaluated using the experimentally measured CM and DM impedance of the cable connected machine winding. The resistance "R_e" in series with the equivalent inductance represents the damping and can be evaluated using the DM impedance measured at 0 Hz. Using the equivalent Π circuit, the CM and DM impedance can be expressed as;

$$Z_{CM} = \frac{2}{C_e} \cdot \frac{s^2 + {}^{R_e}/_{L_e} s + 1 \Big/ \left(\sqrt{{}^{L_e C_e}/_{2}}\right)^2}{s\left(s^2 + {}^{R_e}/_{L_e} s + 2 \Big/ \left(\sqrt{{}^{L_e C_e}/_{2}}\right)^2\right)} \tag{9}$$

$$Z_{DM} = R_e + sL_e \tag{10}$$

The CM impedance exhibits a dominant pole at the origin, whereas the DM impedance is characterized by a dominant zero, assuming negligible resistance. The effect of the dominant pole in the CM impedance is evident in its linear decrease at low frequencies. Conversely, the DM impedance demonstrates a linear increase at low frequencies, attributable to the presence of the dominant zero. It is necessary to increase the impedance at the anti-resonance frequency to dampen the voltage oscillations. If, with the filter connected to the machine, the impedance increases by factor k, then, the equivalent Γ circuit of the filter connected machine can be represented as shown in Fig. 14 (c). Thus, the filter impedance (Z_{filter}), and hence, the filter parameters (R and C) can be calculated using (11-12),

$$Z_{filter} = \frac{1}{\frac{1}{kZ_{CM_0} - \frac{Z_{DM_0}}{2}} - \frac{1}{Z_{CM_0} - \frac{Z_{DM_0}}{2}}} - \frac{Z_{DM_0}}{2} \quad (11)$$

$$R = real(Z_{filter}) \quad (12\text{-a})$$

$$C = -\frac{1}{\omega_{far} \times imag(Z_{filter})} \quad (12\text{-b})$$

By way of example, from Fig. 13, the CM and DM impedance of the machine at the 1st anti-resonance frequency (ω_{far}) is $40.35\angle -22.0$ and $247.0\angle 60.32$ respectively. Using (11-12), the parameters of the filter impedance (Z_{filter}) for increasing the impedance to 100 Ω will be R = 159.2 Ω and C = 4.423 nF. Fig. 15 illustrates the effect of the filter as an increase in the impedance at the anti-resonance frequency. With the filter, the impedance increases from 40.35 Ω to 100 Ω which helps in damping the voltage oscillations at the neutral point.

According to (9-10), the CM and DM impedance depends on the equivalent capacitance, inductance and resistance of the cable connected machine winding. Equivalent capacitance indicates the capacitance between the winding and the core of the machine. For larger machines, the capacitance is high, which lead to lower CM impedance. On the other hand, equivalent inductance represents the series inductance of the cable and the machine winding. As the number of turns in the phase increases, so does the inductance, leading to higher DM impedance. Equivalent resistance is a measure of the resistance of the winding at a given frequency of excitation. At higher frequencies, the resistance of the winding increases due to the skin and proximity effects. As a result, the impedance of the winding at the anti-resonance frequency increases. This higher impedance contributes to greater damping within the system.

V Experimental Validation

The design and effectiveness of the conventional filters in attenuation of the voltage oscillation at the neutral point of a machine winding has been evaluated in the previous section, where, it is illustrated that the conventional filter does not alleviate the neutral point voltage oscillation. In the following section, the effectiveness of the proposed RC filter designed in section IV is experimentally evaluated.

The experimental rig developed to analyze the filter performance is illustrated in Fig. 16, wherein, the filter is installed to a VSI which feeds the stator of a 60 kW PMSM machine used in the 2010 Toyota Prius hybrid vehicle [27]. The cable between the VSI and machine is a 2.5 m long shielded manufactured by LAPP, whose specification is given in [3]. The VSI is a SiC MOSFET-based inverter with 1200 V, 60 A C2M0040120 CREE devices. In the experiments, the voltage at the DC link is 550 V, the rise time of the voltage pulse is 20 ns and the switching frequency is 40 kHz. The PE wire of the cable is connected to the mid-point of the DC link at the inverter end, and to the machine core at the machine end. During the experiment, 1400 V, 100 MHz bandwidth ADP305 Teledyne Lecroy high voltage active differential probes are used to measure the Phase A pole voltage, Phase A machine terminal-to-core voltage, and the neutral point-to-core voltage. The CM current is measured using 30 A, 50 MHz Bandwidth, Teledyne

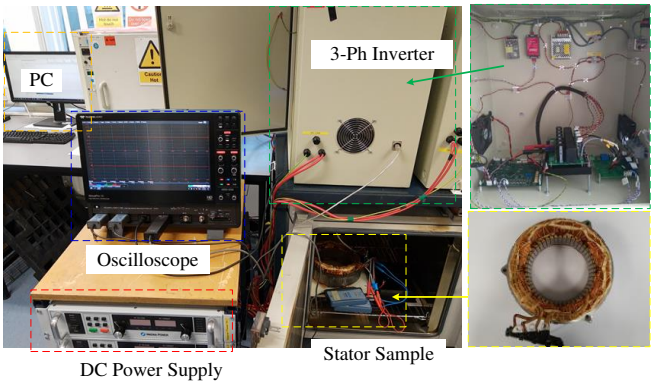

Fig. 16. Experimental rig illustrating stator winding to a three-phase VSI through a 2.5m long shielded cable.

Lecroy CP030 current probe. Without any filter connected to the VSI-fed drive, at a low modulation index and 550 V DC link voltage, Fig. 17 shows the experimentally measured Phase A machine terminal-to-core voltage, neutral point-to-core voltage, and the CM current.

Notably, the peak-to-peak neutral point voltage is 1.4 kV and the CM RMS current is 1.358 A with a peak-to-peak current of 14 A. The CM current is a damped AC current which consists of frequencies corresponding to the voltage stress at the machine terminal and the voltage stress at the neutral point. For instance, Fig. 17 illustrates the CM current flowing through the CM path along with the voltage stress at the neutral point and machine terminal. Notably, the CM current consist of high-frequency component which corresponds to the voltage stress at the machine terminal and a low-frequency component, which corresponds to the voltage stress at the neutral point.

The experimental prototype of the proposed RC filter connected between the neutral and the core of the stator winding is illustrated in Fig. 18. Compared to the theoretically calculated R = 159.18 Ω and C = 4.4233 nF, a 4.7 nF Vishay metalized polypropylene film capacitor and two 330 Ω, 90 W thick film power resistor connected in parallel are used. As illustrated in Fig. 19, after connecting the filter between the neutral point and the core of the machine, the impedance at the anti-resonance frequency is increased to 100 Ω. Further, the anti-resonance frequency shifts to 190 kHz with increased impedance. Thereby, the oscillation frequency reduces from 287.32 kHz to

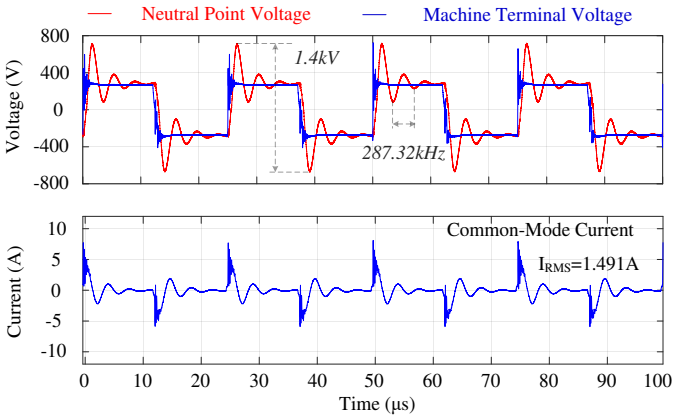

Fig. 17. Experimentally measured voltage stress within winding without filter.

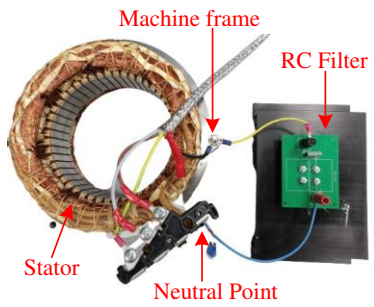

Fig. 18. Experimental prototypes of the proposed RC filter connected to the stator winding.

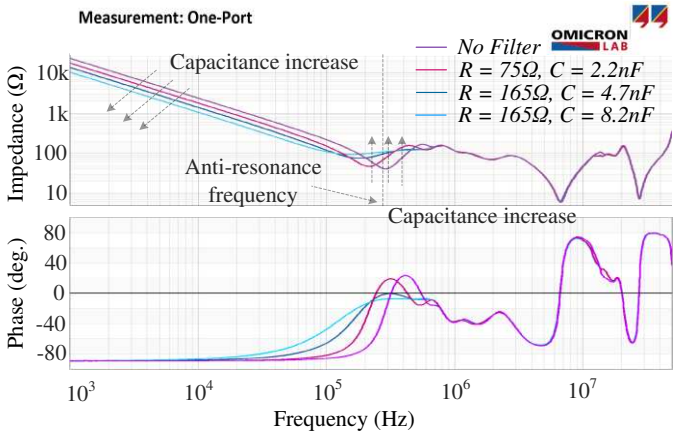

Fig. 19. Experimentally measured CM impedance with a proposed RC filter.

190 kHz with increased damping. From Fig. 20 (a), the peak-to-peak voltage is reduced substantially from 1.4 kV to 903.3 V. The loss incurred by the resistor is 67.18 W, which is merely 0.112 % of the rated power of the machine. The losses are calculated at low modulation index, as the maximum losses are observed at this condition. This attributes to the fact that, at low modulation index, the voltage stress at the neutral point is at maximum, as the voltage waves impinges machine terminal simultaneously and superpose constructively at the neutral point. Increased voltage stress results in higher RMS current flowing through the filter, leading to maximum losses. Additionally, the peak-to-peak CM current reduces from 14 A to 12.37 A. The HF oscillation and its magnitude in CM current depend on the dwell time between the switching of different phases and the parasitic of the VSI which causes a change in its RMS and peak-to-peak.

The experiments are conducted in light load conditions where the CM voltage is the largest resulting in maximum losses. Evidently, from Fig. 19, increasing the capacitance to 8.2 nF, lowers the anti-resonance frequency to 120 kHz, while impedance at anti-resonance increases to 89 Ω. As a result, from Fig. 20 (b), with these parameters, the peak- to-peak neutral point voltage is reduced to 778 V. However, the filter current increases to 0.745 A, and losses to 91.58 W. The current can be reduced to 0.437 A by reducing the capacitance to 2.2 nF, as shown in Fig. 21, but at the expense of higher voltage stress. Increasing the capacitance has two primary effects: (1) It increases the impedance at the anti-resonance frequency,

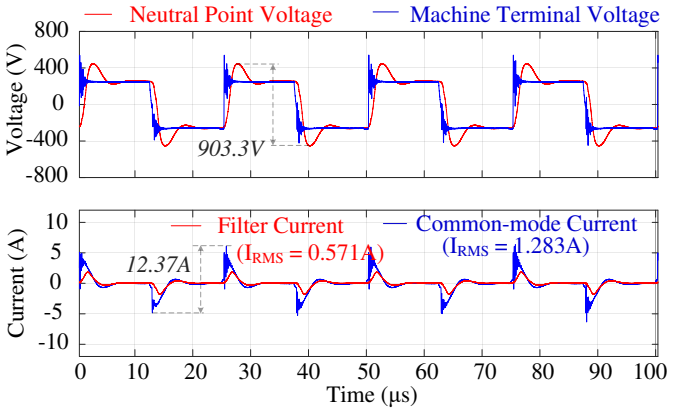

(a)

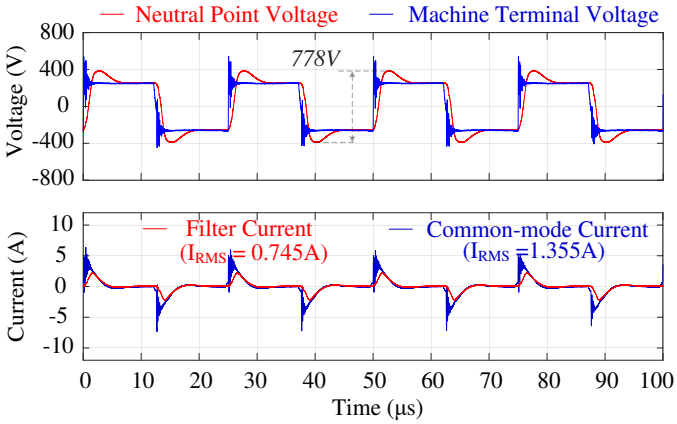

(b)

Fig. 20. Experimentally measured voltage stress with RC Filter; (a) R = 165 Ω, C = 4.7 nF, (b) R = 165 Ω, C = 8.2 nF.

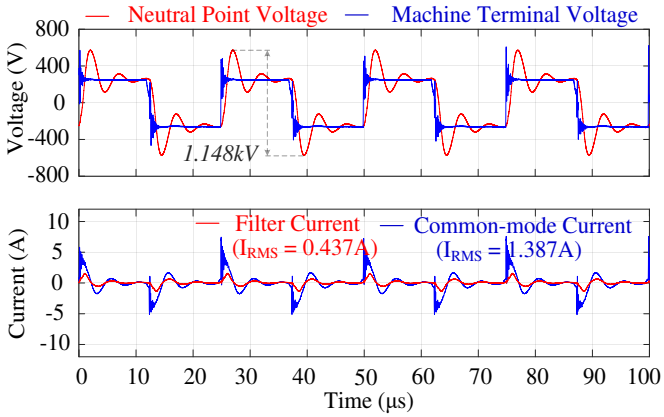

Fig. 21. Experimentally measured voltage stress within winding with RC Filter (R = 75 Ω, C = 2.2 nF).

thereby enhances the damping factor of the voltage oscillation, which leads to its rapid suppression; (2) It decreases the impedance at low frequencies, resulting in a reduction of the impedance of the CM path and causing more losses. Therefore, by increasing the capacitance, the neutral point voltage can be reduced, however, at the expense of additional losses.

For effective suppression, it is essential that the cut-off frequency of the RC filter is set below the first anti-resonance frequency by selecting capacitors with sufficiently high capacitance. However, it is important to note that increased capacitance decreases the impedance in the common-mode

path, which in turn raises the current through the filter and leads to increased losses. The cut-off frequency (ω_c) of the filter, the attenuation (M) at the anti-resonance frequency (ω_{far}) and the impedance of the filter are:

$$\omega_c = \frac{1}{RC} \tag{13}$$

$$M = -10\log\left(1 + \left(\frac{\omega_{far}}{\omega_c}\right)^2\right) \tag{14}$$

$$Z(\omega) = R + \frac{1}{j\omega C} \tag{15}$$

where, R and C are the resistance and capacitance of the filter respectively. According to (13-14), higher capacitance leads to lower cut-off frequency and high attenuation at anti-resonance frequency. However, this leads to low impedance at low frequency which leads to high CM current and incur more losses. For example, with a resistor of 165 Ω and a capacitor of 4.7 nF, the cut-off frequency of the filter is 205.23 kHz, providing an attenuation of -4.71 dB at the first anti-resonance frequency. Conversely, when the capacitance is increased to 8.2 nF, the cut-off frequency decreases to 117.63 kHz, and the attenuation improves to -8.43 dB. However, this increased capacitance also reduces the CM impedance, which results in a higher CM current. The primary criterion in designing such a filter is to minimize voltage stress while keeping losses to a minimum. However, a trade-off exists between the voltage stress and the losses, meaning that reducing one typically results in an increase in the other. The resistive losses can be minimized by reducing the capacitance and the resistance. By way of example, when R=75 Ω and C = 2.2 nF, the loss reduces to 14.32 W. However, the peak-to-peak voltage stress soars to 1.148 kV. This occurs as a result of low impedance at anti-resonance frequency which is illustrated in Fig. 19. During experiments, 9 different RC filter parameter combinations were assessed to explore the best solution which losses. Combination of three different R and C, i.e., R = 75 Ω, 165 Ω, and 340 Ω, and C = 2.2 nF, 4.7 nF, and 8.2 nF were examined. The comparison between the filters against the losses, filter RMS current, and the peak-to-peak neutral point voltage stress is outlined in Fig. 22. The least voltage stress occurs when R = 165 Ω and C = 8.2 nF, conducive to the increased service life of the machine. However, the filter losses increase to 91.58 W. The least loss occurs when R = 75 Ω and C = 2.2 nF. However, with this parameter, the filter is ineffective in damping the voltage oscillations, as the peak-to-peak voltage stress reaches 1.148 kV. The optimum solution of the filter is with R = 165 Ω and C = 4.7 nF, as calculated analytically (11-12), wherein the voltage stress is low with lower losses.

VI Discussions

The conventional filters are ineffective in attenuating the voltage stress at the neutral point. Indeed, they are efficacious in mitigating the terminal voltage stress as discussed in detail in the literature [11-14]. However, when the resonance frequency of the filter is less than the 1st anti-resonance frequency of the winding, a dV/dt filter can partially mitigate the neutral stress at the expense of increased size and cost.

By way of example, Fig. 23 (a) shows a Schaffner FN510 dV/dt filter [28] whose schematic is shown in Fig. 23 (b). The filter is selected appropriately according to the voltage and power rating of the drive under study. As can be seen, the capacitance and inductance of the filter are much greater than those designed according to [11]. The measured CM impedance of the filter is shown in Fig. 24. Evidently, the resonance frequency of the filter is 137.16 kHz, which is lower than the combined anti-resonance frequency of the cable and machine winding (287.32 kHz). Consequently, it increases the impedance at the anti-resonance frequency of the combined filter, cable, and machine winding.

When this filter is connected in between the VSI and the

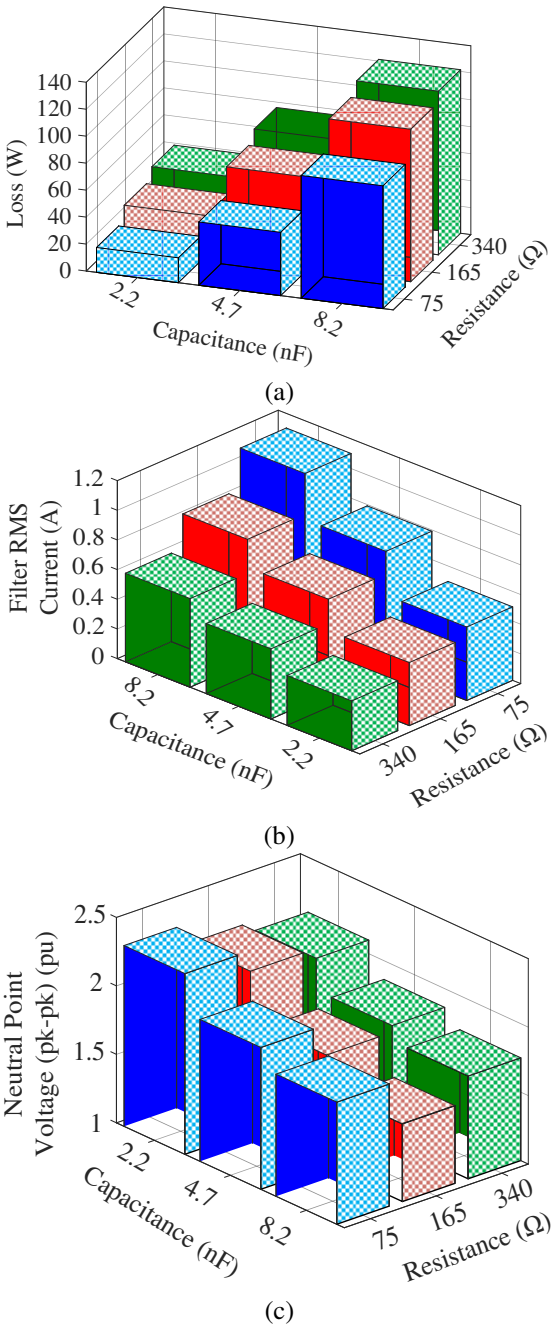

Fig. 22. Comparison between RC filter with different parameters based on; (a) Filter power loss, (b) Filter RMS current, (c) Neutral point voltage stress.

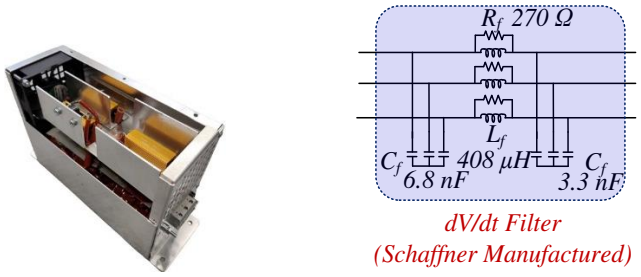

(a) (b)

Fig. 23. Schaffner dV/dt Filter [28]; (a) Actual filter, (b) Schematic of the filter.

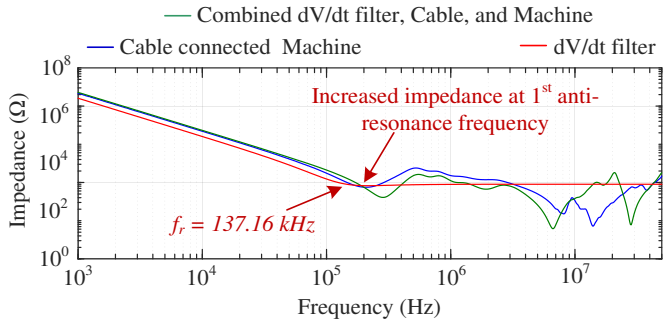

Fig. 24. Experimentally measured CM impedance with dV/dt filter [28].

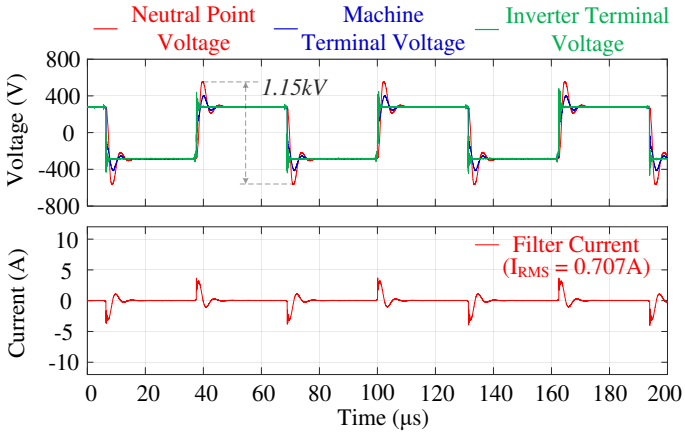

Fig. 25. Experimentally measured voltage stress within winding with dV/dt filter [28].

cable, the peak-to-peak neutral point voltage reduces to 1.15 kV (17.85 % reduction) with a 50 % reduction in CM RMS current as well as a 33 % reduction in the peak-to-peak machine terminal voltage, as illustrated in Fig. 25. However, compared to the RC filter, the peak-to-peak voltage stress at the neutral point is 27.31 % higher while the cost and the footprint of the filter are significantly higher. Thus, the neutral point voltage stress can be partially mitigated by the dV/dt filter, at the expense of increased size, weight, and cost. The difference in the characteristics of the voltage oscillation demands filters with different characteristics. Without any filter, the peak-to-peak voltage stress is 1.4 kV, This stress reduces by 17.85 % to 1.15 kV upon connecting the dV/dt filter, as illustrated in Fig. 26.

Thus, the dV/dt filter suppresses the terminal end voltage effectively and provides partial attenuation of the neutral point

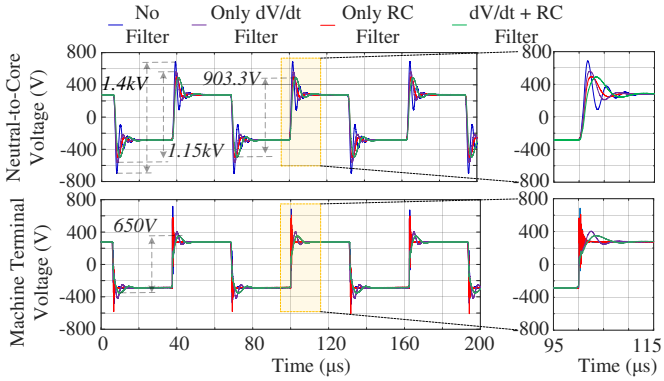

Fig. 26. Experimentally measured neutral point voltage stress with different filters.

TABLE I
A COMPARATIVE STUDY BETWEEN THE PERFORMANCE OF DIFFERENT TYPES OF PASSIVE FILTERS

Performance Criteria	Sinewave Filter [13]	dV/dt Filter [11]	dV/dt Filter [28]	Proposed Filter
Voltage drop	4-10 %	0.5 %	1 %	0 %
Neutral point voltage stress (p.u.)	1.22	1.14	0.82	0.65
CM current (RMS) (A)	0.5	1.4	0.71	1.28
Loss	10 %	2.5 %	5 %	0.112 %
Cost ($/unit)	$ 783	$ 304	$ 368	$ 80
Footprint size (mm^2)	200×145	150×90	260×85	38×30.9

overvoltage. In contrast, the proposed RC filter suppresses the neutral point voltage significantly and provides marginal attenuation of the terminal end voltage. The benefits of each can be combined when both filters are used at the same time. When both the filters are connected, the peak-to- peak neutral point voltage is reduced to 903.3 V and the peak- to-peak voltage stress at the machine terminal is reduced to 650 V. The voltage overshoot at the machine terminal is reduced to 1.18 pu. Therefore, the combination of the dV/dt filter and the RC filter is an optimal solution for suppressing the peak voltage stress, resulting in a reduced likelihood of premature failure.

Indeed, for effective voltage stress suppression, the corner frequency of the filter should be selected to be lower than the 1st anti-resonance frequency. The lower the 1st anti-resonance frequency is, the bigger the size of the magnetic component of the filter.

A comparative analysis between the performance of different filters is provided in Table I. The comparison shows that the proposed RC filter effectively attenuates the new mode of voltage stress at the neutral point without significant increase in loss, cost and without any magnetic component.

VII CONCLUSION

This work proposes a low-cost, passive RC filter to reduce voltage stress at the neutral point in VSI-fed drive systems, an

aspect often overlooked despite existing studies and standards. This study shows that while traditional filters like sinewave filters can lower voltage stress at the machine terminal, they might actually increase stress at the neutral point. The dV/dt filters can help reduce stress, but they must have a resonance frequency lower than the combined cable and machine's anti-resonance frequency. However, this often leads to a costly and bulky solution due to the required large magnetic components.

The proposed RC filter is effective in alleviating the voltage stress at the neutral point while incurring small additional losses. The design of the RC filter requires a trade-off between the voltage stress and the filter losses. This study proposes an analytical approach, based on impedance measurement, to select the optimal parameters of the filter. The proposed filter offers an inexpensive and compact solution that can be easily embedded in electrical machines. Although the suggested passive filter effectively reduces voltage stress at the neutral point, it is ineffectual at reducing voltage stress at the machine terminals. Therefore, the proposed filters should be used in conjunction with conventional filters to provide a complete solution for voltage stress mitigation in electrical machines.

For future work, the study could extend to multi-objective optimization of the proposed filter while minimizing voltage stress, common-mode current, and losses.

ACKNOWLEDGMENT

The authors acknowledge the support from the project partner, Dr Mohamed Diab, Dr. Ian Laird and Prof. Xibo Yuan from The University of Bristol for the provision of the SiC inverter used in the experiments.

REFERENCES

[1] A. Hoffmann and B. Ponick, “Method for the prediction of the potential distribution in electrical machine windings under pulse voltage stress,” *IEEE Trans. Energy Convers.*, vol. 36, no. 2, pp. 1180-1187, June 2021.

[2] J. M. MartÍnez-Tarifa, H. AmarÍs-Duarte and J. Sanz-Feito, “Frequency-domain model for calculation of voltage distribution through random wound coils and its interaction with stray capacitances,” *IEEE Trans. Energy Convers.*, vol. 23, no. 3, pp. 742-751, Sept. 2008.

[3] S. Sundeep, J. Wang and A. Griffo, “Holistic modeling of high-frequency behavior of inverter-fed machine winding, considering mutual couplings in time domain,” *IEEE Trans. Ind. Appl.*, vol. 57, no. 6, pp. 6044-6057, Nov.-Dec. 2021.

[4] S. Sundeep, J. Wang, A. Griffo and F. Alvarez-Gonzalez, “Antiresonance phenomenon and peak voltage stress within PWM inverter fed stator winding,” *IEEE Trans. Ind. Electron.*, vol. 68, no. 12, pp. 11826-11836, Dec. 2021.

[5] H. Akagi and S. Tamura, “A passive EMI filter for eliminating both bearing current and ground leakage current from an inverter-drive motor,” *IEEE Trans. Power Electron.*, vol. 21, no. 5, pp. 1459–1469, Sep. 2006.

[6] G. L. Skibinski, R. J. Kerkman, and D. Schlegel, “EMI emissions of modern PWM ac drives,” *IEEE Ind. Appl. Mag.*, vol. 5, no. 6, pp. 47–80, Nov./Dec. 1999.

[7] T. Plazenet, T. Boileau, C. Caironi and B. Nahid-Mobarakeh, “Influencing parameters on discharge bearing currents in inverter-fed induction motors,” *IEEE Trans. Energy Convers.*, vol. 36, no. 2, pp. 940-949, June 2021.

[8] S. Chen, T. A. Lipo and D. Fitzgerald, “Source of induction motor bearing currents caused by PWM inverters,” *IEEE Trans. Energy Convers.*, vol. 11, no. 1, pp. 25-32, March 1996.

[9] F. J. T. E. Ferreira, M. V. Cistelecan and A. T. de Almeida, “Evaluation of slot-embedded partial electrostatic shield for high-frequency bearing current mitigation in inverter-fed induction motors,” *IEEE Trans. Energy Convers.*, vol. 27, no. 2, pp. 382-390, June 2012.

[10] A. F. Moreira, P. M. Santos, T. A. Lipo and G. Venkataramanan, “Filter networks for long cable drives and their influence on motor voltage distribution and common-mode currents,” *IEEE Trans. Ind. Electron.*, vol. 52, no. 2, pp. 515-522, April 2005.

[11] S. Baek, Y. Cho, B. Cho and C. Hong, “Performance comparison between two-level and three-level SiC-based VFD applications with output filters,” *IEEE Trans. Ind. Appl.*, vol. 55, no. 5, pp. 4770-4779, Sept.-Oct. 2019.

[12] J. He, G. Y. Sizov, P. Zhang and N. A. O. Demerdash, “A review of mitigation methods for overvoltage in long-cable-fed PWM AC drives,” in *Proc. IEEE Energy Conversion Congress and Exposition (ECCE)*, Arizona, USA, pp. 2160-2166, 2011.

[13] P. Mishra and R. Maheshwari, “Design, analysis, and impacts of sinusoidal LC filter on pulsewidth modulated inverter fed-induction motor drive,” *IEEE Trans. Ind. Electron.*, vol. 67, no. 4, pp. 2678-2688, April 2020.

[14] M. Kumar and J. Kalaiselvi, “Analysis and measurement of non-intrinsic differential-mode noise in a SiC inverter fed drive and its attenuation using a passive sinusoidal output EMI filter,” *IEEE Trans. Energy Convers.*, vol. 38, no. 1, pp. 428-438, March 2023.

[15] D. Graovac, T. Hoffmann and A. Haltmair, “A transfer function approach to a common mode filter (CMMF) optimization in the PWM inverter supplied motor drives,” *IEEE Trans. Energy Convers.*, vol. 26, no. 1, pp. 93-101, March 2011.

[16] J. Xue, F. Wang, and W. Chen, “A study of motor-end EMI filter on output common-mode noise suppression in DC-fed motor drive system,” in *Proc. 28th Annu. IEEE Appl. Power Electron. Conf. Expo. (APEC)*, Indonesia, pp. 1556–1561, March 2013.

[17] C. Mei, J. Balda and W. Waite, “Cancellation of common-mode voltages for induction motor drives using active method,” *IEEE Trans. Energy Convers.*, vol. 21, no. 2, pp. 380-386, June 2006.

[18] Z. Lyu and L. Wu, “Resonant frequency deviation analysis and modified notch filter-based active damping for SiC-based PMSM drive with sine wave filter,” *IEEE Trans. Energy Convers.*, vol. 38, no. 1, pp. 417-427, March 2023.

[19] Motors and Generators, NEMA MG1–2021 Part 31, 2021.

[20] Rotating electrical machines-Part 25: Guidance for the design and performance of a.c. motors specifically designed for converter supply, IEC 60034- 25:2022, 2022.

[21] Adjustable speed electrical power drive systems-Part 8: Specification of voltage on the power interface, IEC 61800-8:2010, 2010.

[22] S. De, K. Hatua, M. M. R. Rajne, “Common mode filter motor controllers”, US 8115444B2, Feb. 14, 2012. Available: https://patents.google.com/patent/US8115444B2/en, Accessed on: April 22, 2024.

[23] S. Schroth, R. Oberst, M. Pils, M. Weckert, “Device for avoiding harmful bearing current”, DE 102015112146A120170126, Jan. 01, 2017.

[24] D. Zhang, T. Fan, P. Ning and X. Wen, “An automatic EMI filter design methodology for electric vehicle application,” *in Proc. IEEE Energy Conversion Congress and Exposition (ECCE), Cincinnati, Ohio, USA*, pp. 4497-4503, 2017.

[25] L. Zhai, G. Hu, C. Song, M. Lv and X. Zhang, “Comparison of two filter design methods for conducted EMI suppression of PMSM drive system for electric vehicle,” *IEEE Trans. Vehicular Tech.*, vol. 70, no. 7, pp. 6472-6484, July 2021.

[26] B. Wu, M. Narimani, *High-Power Converters and AC Drives*, 2nd ed., Hoboken, New Jersey, John Wiley & Sons, Inc., 2017.

[27] M. Olszewski (2011 March). Evaluation of the 2010 Toyota Prius hybrid synergy drive system. Oak Ridge National Laboratory, USA. [Online] Available: https://info.ornl.gov/sites/publications/files/pub26762.pdf, Accessed on: Jan. 2024.

[28] Datasheets, Schaffner Group, pp 1-4 [Online] Available: https://www.mouser.co.uk/datasheet/2/355/fn-510-1036165.pdf Accessed on: Jan. 2024.

BIOGRAPHIES

Shubham Sundeep is a Postdoctoral Researcher at the National Renewable Energy Laboratory (NREL), USA. Shubham holds a Ph.D. in electronic and electrical engineering from the University of Sheffield, UK, awarded in 2022. He also earned an M.Tech. in power electronics, electrical machines and drives from the Indian Institute of Technology (IIT) Delhi, India, in 2017.

His research focuses on high-frequency modeling, condition monitoring, diagnostics, control and operation of electric drives, and drivetrain design for mechanical energy storage systems. Prior to joining NREL, Shubham worked as an Engineer at EATON Corporation, where he developed synchronous drive control systems. At IIT Delhi, he developed a novel sensorless control technique for permanent magnet BLDC motors. His doctoral research at the University of Sheffield advanced the understanding of wideband-gap semiconductor devices and their impacts on electric drives. Shubham has authored 19 peer-reviewed publications, including six IEEE Transactions, one IET Journal, and twelve conference papers in IEEE and IET. He has also presented his research at numerous international conferences. His paper on high-frequency modeling of electrical machines won the 2nd Prize Paper Award from the IEEE Industrial Drives Committee in the IEEE Industry Applications Society, in 2021.

Jiabin Wang received the B.Eng. and M.Eng. degrees from Jiangsu University, Zhengjiang, China, in 1982 and 1986, respectively, and the Ph.D. degree from the University of East London, London, U.K., in 1996, all in electrical and electronic engineering.

From 1986 to 1991, he was with the Department of Electrical Engineering, Jiangsu University, appointed a Lecturer in 1987 and an Associate Professor in 1990. He was a Postdoctoral Research Associate at the University of Sheffield, from 1996 to 1997, and a Senior Lecturer at the University of East London from 1998 to 2001. He was with the Electrical Machines and Drives Group at the University of Sheffield as a Senior Lecturer from 2001 to 2006, a Reader from 2007 to 2010, and a Professor of Electrical Engineering from 2010 to 2023. He is currently an Emeritus Professor at the University of Sheffield, Sheffield, U.K. His research interests encompass novel rotary and linear electrical machines and drives, advanced control techniques for electrical drives, and electrical power-train technologies with a particular focus on high integrity, fault-tolerant, and high-efficiency electric drives and associated condition monitoring techniques for applications in aerospace, automotive and renewable energy systems

Antonio Griffo (Member, IEEE) received the M.Sc. degree in electronic engineering and the Ph.D. degree in electrical engineering from the University of Naples "Federico II," Naples, Italy, in 2003 and 2007, respectively. From 2007 to 2013, he was a Research Associate with The University of Sheffield, Sheffield, U.K., and the University of Bristol, Bristol, U.K. He is currently a Professor with the School of Electrical and Electronic Engineering, The University of Sheffield. His research interests include design, control, and condition monitoring of electric power systems, power electronics converters, and electrical motor drives for renewable energy, automotive, and aerospace applications. Dr. Griffo is an Associate Editor of IEEE TRANSACTIONS ON INDUSTRIAL ELECTRONICS.